ACS Energy LETTERS

http://pubs.acs.org/journal/aelccp

LETTER

# *Ab Initio* Thermodynamics and Kinetics of the Lattice Oxygen Evolution Reaction in Iridium Oxides

Alexandra Zagalskaya,[¶] Iman Evazzade,[¶] and Vitaly Alexandrov*

Cite This: *ACS Energy Lett.* 2021, 6, 1124–1133

Read Online

ACCESS | Metrics & More | Article Recommendations | Supporting Information

**ABSTRACT:** **Iridium-oxide-based catalysts are among the most active and stable materials for the anodic oxygen evolution reaction (OER) in acidic media, but even their longevity represents an important issue. It was recently demonstrated for many transition-metal oxides that stability of a catalyst can suffer from the active participation of lattice oxygen atoms in the OER. In this work, we combine density functional theory-based thermodynamics and molecular dynamics to analyze the OER activity of a series of Ir-bearing oxides. We reveal that although some Ir oxides exhibit thermodynamic overpotentials lower than that of the state-of-the-art $IrO_2$ rutile for the conventional reaction pathway, they also feature concomitant activation of lattice oxygen atoms toward the OER. By focusing on a few representative cases we unequivocally demonstrate that the lattice oxygen mechanism can outperform the conventional mechanism owing to its lower kinetic barriers. As lattice oxygen evolution was experimentally correlated with oxide degradation, enhanced OER activity due to involvement of lattice oxygen should compromise materials stability. This study highlights the importance of considering the lattice oxygen evolution reaction for more reliable computational predictions of electrochemically stable OER catalysts.**

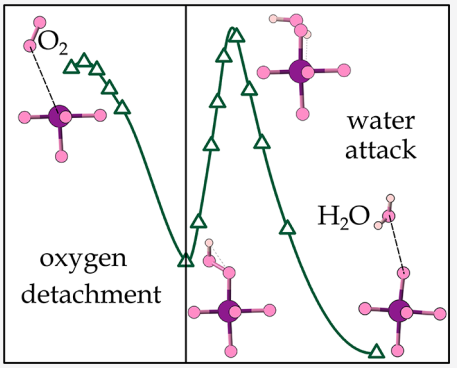


Electrocatalytic water splitting to produce $H_2$ and $O_2$ is a promising strategy to utilize renewable energy.[1−7] In recent years great effort has been directed at designing new catalytically active materials for both the cathodic (hydrogen evolution reaction, HER) and anodic (oxygen evolution reaction, OER) half-reactions of electrochemical water splitting. The OER half-reaction has received major attention as a kinetically more sluggish process determining the overall performance of water electrolyzers. In addition to exhibiting great activity, the best HER/OER electrocatalysts should also be highly stable under reaction conditions. Therefore, the past few years have seen an upsurge of interest in identifying durable water-splitting electrocatalysts[2,8−10] alongside with developing strategies to mitigate material degradation.[11−13]

*Ab initio* based high-throughput screening calculations offer an efficient way to discover catalysts with desired combinations of activity and stability properties. One of the theoretical schemes to analyze materials' stability as a function of aqueous conditions such as pH and electrode potential is the construction of computational Pourbaix diagrams.[14] This approach has been widely applied to predict the aqueous stability of a variety of materials including those to be used for acidic OER electrocatalysis, such as Ir- and Ru-based oxides.[15−17] For instance, in a recent density functional theory (DFT)-based study employing an active-learning accelerated algorithm coupled with a Pourbaix Ir−$H_2O$ analysis, more than 38 000 structural candidates have been screened to discover the most promising Ir-oxide polymorphs such as $\alpha$-$IrO_3$.[18] The other computational investigation in conjunction with a Pourbaix stability analysis has focused on screening equimolar bimetallic $IrO_2$-based systems to identify OER-active and acid-stable catalysts with lower Ir content, such as Co−Ir, Fe−Ir, and Mo−Ir oxides.[17] Such computational screenings of large crystal structure libraries are typically done by evaluating theoretical thermodynamic overpotentials ($\eta_{OER}$) for the conventional OER mechanism.[6,16,17,19−22] This mechanism is often termed the adsorbate evolving mechanism (AEM) as it is composed of four concerted electron−proton transfer steps involving oxygen intermediates adsorbed over a transition-metal surface site.

**Received:** February 1, 2021
**Accepted:** February 25, 2021
**Published:** March 2, 2021

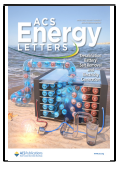







https://dx.doi.org/10.1021/acsenergylett.1c00234
*ACS Energy Lett.* 2021, 6, 1124−1133

Recently, however, a series of investigations have revealed that OER in a multitude of transition-metal oxides can also proceed via direct formation of $O_2$ from the lattice oxygen atoms, commonly termed the lattice oxygen mechanism (LOM).[5,7,23] Moreover, the observed high OER activities are often rationalized in terms of lattice oxygen participation for many oxides, such as $LaNiO_{3-\delta}$,[24−26] $SrCoO_{3-\delta}$,[27,28] $La_{1-x}Sr_xCoO_{3-\delta}$,[29,30] and (Co,Zn)OOH.[31] However, such enhanced activities typically come at the expense of decreased stability as LOM has been associated with substantial surface reconstruction, cationic migration to the surface, and eventual dissolution.[24,32−34] For instance, the atomic-scale structure of Ir-oxide catalysts has been recently correlated with the extent of lattice oxygen involvement in the OER that results in oxide degradation.[35] In particular, it has been proposed that a lower stability of hydrous $IrO_x$ relative to rutile $IrO_2$ can be attributed to a greater concentration of electrophillic $O^{I-}$ anions in $IrO_x$ due to the high number of defects. These electrophilic oxygen sites are hypothesized to serve as active centers for nucleophilic attack by water weakening the connectivity between $IrO_6$ octahedra in the lattice and triggering dissolution of Ir.[35,36] The high porosity of hydrous $IrO_x$ is believed to be also beneficial for LOM by making lattice oxygen atoms more accessible for water attack.

Even in the case of exceptionally stable rutile $IrO_2$ a recent experimental investigation has been able to quantify the lattice oxygen involvement in OER by using sufficiently sensitive experimental techniques.[37] Through a combination of isotope labeling and atom probe tomography, the lattice oxygen exchange has been not only detected but also quantitatively correlated with the amount of dissolved Ir. It has been estimated that one Ir atom is dissolved per approximately 33 exchanged lattice oxygen atoms. These results are in qualitative agreement with our previous DFT thermodynamics study showing that metal vacancies promote LOM in rutile-type $RuO_2$ and $IrO_2$.[38]

Observations of the lattice oxygen participation in OER across various transition-metal oxides are consistent with a more general thermodynamic analysis correlating OER and corrosion of oxide catalysts.[39] The study has demonstrated that any metal oxide must become destabilized under the highly oxidizing conditions of the OER because of the thermodynamic instability of oxygen atoms in the metal oxide lattice. Note that this key aspect is not captured by stability analyses carried out using Pourbaix diagrams because of their assumption of complete thermodynamic equilibrium for the oxygen partial pressure. The observed interplay between activity and stability in oxygen electrocatalysis bears a close resemblance with the field of high-energy Li-ion batteries. It is now established that not only cationic but also anionic redox reactions in many oxide cathodes can contribute to the energy storage capacity, while the lattice oxygen evolution reaction may lead to irreversible capacity loss.[40−43] Therefore, it is crucial to deeply understand the role of lattice oxygen evolution and its effect on oxide stability across a variety of systems under different electrochemical conditions.

In this computational study, we investigate OER energetics of the AEM and LOM mechanisms across a number of Ir-based oxides and compare it with the benchmark rutile-structured $IrO_2$ polymorph. Our choice of iridium oxides here is based on recent theoretical predictions of high AEM activity for several $IrO_2$, $IrO_3$, as well as bimetallic Ir-bearing oxide phases. The objective of the study is twofold. First, we wish to demonstrate that the high AEM activity is concurrent with activation of lattice oxygen atoms in the studied oxides, suggesting a strong correlation between surface activity and stability. Second, we aim to show that LOM can indeed outperform AEM as predicted by DFT-based thermodynamic and kinetic simulations. Thus, in addition to computing OER overpotentials we also evaluate free energy barriers for the two representative LOM pathways previously hypothesized in the literature (involving O−O coupling and nucleophilic water attack) through *ab initio* molecular dynamics (AIMD) and contrast the obtained results with the AEM case. Because of the significance of the dynamic nature of oxide surfaces under OER conditions, we examine OER energetics for both perfect and defective (with Ir vacancies) surfaces. To this end, we employ spin-polarized DFT calculations using the revised Perdew−Burke−Ernzerhof (RPBE) exchange−correlation functional[44,45] in combination with projector augmented wave (PAW) potentials using the VASP code.[46,47] All computational details are provided in the Supporting Information.

Even though the electrolysis of water has been known since the early 19th century, we still keep discovering key mechanistic details about the process. The dominant framework to study the anodic part of electrochemical water splitting (the oxygen evolution reaction, OER) has been the conventional adsorbate-evolving mechanism (AEM).[19,48] According to this mechanism, OER proceeds via a series of four proton-coupled electron transfers over the same metal site on the surface of the electrocatalyst as follows:

$$* + H_2O \rightarrow HO* + e^- + H^+ \quad (1)$$

$$HO* \rightarrow O* + e^- + H^+ \quad (2)$$

$$H_2O + O* \rightarrow HOO* + e^- + H^+ \quad (3)$$

$$HOO* \rightarrow O_2(g) + e^- + H^+ + * \quad (4)$$

Computationally, OER is commonly investigated in the framework of the computational hydrogen electrode (CHE) approach.[19,48] The method enables an evaluation of the thermodynamic overpotential for the overall OER from first-principles as

$$\eta_{OER} = \max[\Delta G_1, \Delta G_2, \Delta G_3, \Delta G_4]/e - 1.23\ V \quad (5)$$

where $\Delta G_i$ ($i$ = 1, 2, 3, 4) are the calculated free energies of the AEM reaction steps and 1.23 V is the equilibrium potential of water splitting. This has become the major approach for computational screening across many material classes to identify highly OER-active catalysts. An important feature of the AEM mechanism is the existence of linear scaling relationships between adsorption energies of the reaction intermediates due to the involvement of only a single active site.[49] This sets a fundamental limit on the catalytic activity of materials calling for strategies aimed to break the linear scaling relationships in order to further reduce the OER overpotential.

Over the past years, however, our understanding of the OER process has expanded to include other mechanisms of oxygen evolution at the catalyst/water interface.[5−7,21] Interestingly, it was demonstrated that oxygen molecules can also evolve directly from the lattice oxygen atoms of a metal-oxide catalyst, termed the lattice oxygen mechanism (LOM).[5,7,23] Moreover, even for the LOM process different reaction pathways were suggested in the literature.[7] These proposed LOM mechanisms


https://dx.doi.org/10.1021/acsenergylett.1c00234
ACS Energy Lett. 2021, 6, 1124−1133

can be grouped into two main classes: the one involving O−O coupling (denoted as LOM1 in Scheme 1) and the other involving water attack similar to the conventional AEM but occurring at the lattice oxygen site (denoted as LOM2 in Scheme 1). It was hypothesized that the mononuclear LOM1 pathway could be kinetically more sluggish than LOM2 as it proceeds via a very strained transition state.[33] We note, however, that analogously to AEM,[6,21,50] binuclear LOM1 reaction pathways can be envisioned. In fact, although we focus here on the mononuclear version of LOM1 as shown in Scheme 1, we did observe spontaneous LOM1 with O−O coupling involving two neighboring Ir sites when modeling defective $\alpha$-$IrO_3$, as alluded to below.

**Scheme 1. Schematic Showing Two Major Mechanisms of the Lattice Oxygen Participation in the OER**[a]

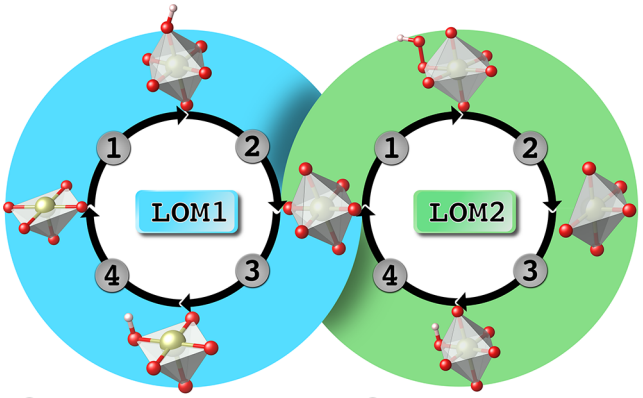


| | LOM1 | LOM2 |
|---|---|---|
| 1 | $* + H_2O = *OH + e^- + H^+$ | $*O_{lat} + H_2O = *O_{lat}OH + e^- + H^+$ |
| 2 | $*OH = *O + e^- + H^+$ | $*O_{lat}OH = *O_{2(g)} + e^- + H^+$ |
| 3 | $*O + O_{lat} = *O_{2(g)} + V_O$<br>$V_O + H_2O = *H + e^- + H^+$ | $V_O + H_2O = *O_{lat}H + e^- + H^+$ |
| 4 | $*H = * + e^- + H^+$ | $*O_{lat}H + *O_{lat} = *O_{lat} + e^- + H^+$ |

[a]LOM1 involves the O−O coupling at the same metal center, whereas LOM2 assumes the nucleophilic water attack similarly to the conventional adsorbate-evolving mechanism (AEM). LOM1 with the O−O coupling involving two neighboring metal sites (bi-nuclear version) is discussed in the text as it was also observed in our simulations. Note that in this scheme the formation of $O_2$ corresponds to step 3 for LOM1 and to step 2 for LOM2.

The conventional AEM mechanism assumes that the reaction occurs at the surface metal center without breaking lattice metal−oxygen bonds. This should result in a less significant effect on surface reorganization. In contrast, LOM might severely compromise the integrity of the oxide lattice by breaking structural metal−oxygen bonds. The formed structural oxygen vacancies as a result of LOM, however, can be healed if they are filled by dissociated water species or diffusing lattice oxygen atoms that can minimize surface restructuring. A quantitative analysis of the role of these processes in surface stability of metal oxides is beyond the scope of the present work. We note, however, that we did not observe any spontaneous vacancy healing during our AIMD simulations. In this study we distinguish the AEM active site as the one involving a terminal surface oxygen atom and the LOM site as the one connecting at least two metal centers in the perfect (nondefective) structure. These active sites are referred to as $O_{cus}$ (AEM site) and $O_{lat}$ (LOM site) throughout the paper and are depicted in Figure 1 for the investigated $IrO_2$ and $IrO_3$ surfaces.

We first analyze the thermodynamics of the AEM and LOM reaction pathways for ideal $IrO_2$ and $IrO_3$ surfaces shown in Figure 1. The computed reaction free energies and the corresponding OER overpotentials are listed in Table 1. In agreement with our previous results for AEM and LOM1 in rutile-structured $IrO_2$,[38] AEM appears to be a much more thermodynamically favorable reaction pathway of the OER. In the rutile case LOM1 is characterized by a much higher overpotential, whereas LOM2 reaction intermediates turn out to be unstable for the considered regular (110) surface. These theoretical results are in line with a low activity of the rutile polymorph toward LOM and its superior stability under the OER conditions.[37]

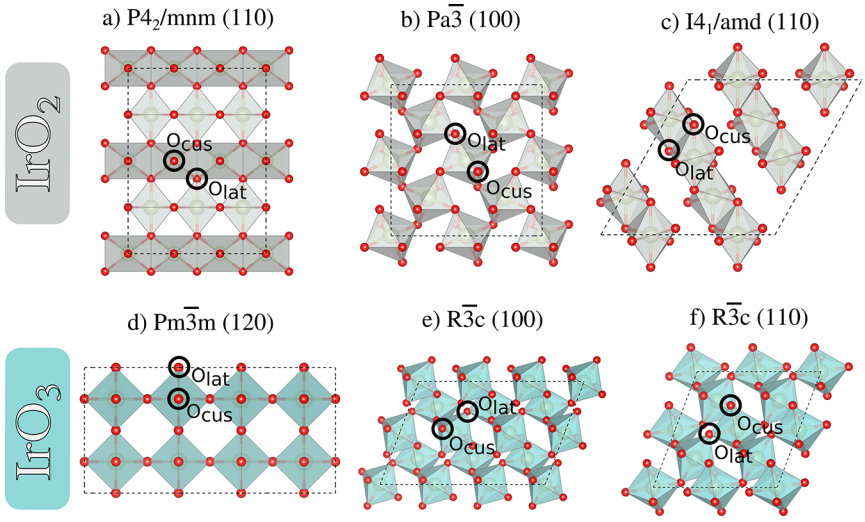


**Figure 1. Top views of the simulation cells used to model the AEM and LOM reaction pathways. Crystal structures of $IrO_2$ (gray polyhedral representation) and $IrO_3$ (teal polyhedral represenation) polymorphs are shown according to their space groups: (a) rutile $IrO_2$ ($P4_2/mnm$), (b) pyrite $IrO_2$ ($Pa\bar{3}$), (c) anatase $IrO_2$ ($I4_1/amd$), (d) $IrO_3$ ($Pm\bar{3}m$), and (e and f) $\alpha$-$IrO_3$ ($R\bar{3}c$). $O_{cus}$ stands for the oxygen sites over the Ir CUS (coordinatively unsaturated) centers participating in AEM, and $O_{lat}$ stands for the lattice oxygen sites involved in LOM. The dashed lines denote surface supercells.**



https://dx.doi.org/10.1021/acsenergylett.1c00234
ACS Energy Lett. 2021, 6, 1124−1133

Table 1. DFT-Calculated Free Energies ($\Delta G_i$, in eV) and Theoretical Overpotentials ($\eta$, in V) for the Ideal $IrO_2$ and $IrO_3$ Surfaces[a]

| structure | mechanism | $\Delta G_1$ | $\Delta G_2$ | $\Delta G_3$ | $\Delta G_4$ | $\eta$ |
|---|---|---|---|---|---|---|
| $P4_2/mnm$ (110) | AEM | 0.00 | 1.29 | 1.65 | **1.99** | 0.76 |
| | LOM1 | | | **3.98** | −0.35 | 2.75 |
| | LOM2 | | | * | | |
| $Pa\bar{3}$ (100) | AEM | 0.45 | 1.41 | 1.52 | **1.54** | 0.31 |
| | LOM1 | | | **2.04** | 1.02 | 0.81 |
| | LOM2 | **2.33** | 1.59 | 0.06 | 0.95 | 1.10 |
| $I4_1/amd$ (110) | AEM | 0.70 | 1.38 | **1.45** | 1.40 | 0.22 |
| | LOM1 | | | **1.82** | 1.02 | 0.59 |
| | LOM2 | **2.07** | 1.84 | 0.05 | 0.96 | 0.84 |
| $R\bar{3}c$ (100) | AEM | **1.45** | 1.36 | 1.38 | 0.72 | 0.22 |
| | LOM1 | | | 0.73 | 1.37 | 0.22 |
| | LOM2 | **3.13** | −0.08 | 1.35 | 0.52 | 1.90 |
| $R\bar{3}c$ (110) | AEM | 0.79 | **1.45** | 1.34 | 1.34 | 0.22 |
| | LOM1 | | | **1.56** | 1.12 | 0.33 |
| | LOM2 | **2.67** | 1.10 | 0.39 | 0.76 | 1.44 |
| $Pm\bar{3}m$ (120) | AEM | **1.76** | 1.27 | 1.56 | 0.34 | 0.53 |
| | LOM1 | | | 1.11 | 0.79 | 0.53 |
| | LOM2 | | | * | | |

[a]The sequence of the OER steps corresponds to Scheme 1. The potential-determining step (PDS) in each case is highlighted in bold. * denotes the cases for which the LOM2 reaction intermediates were found to be unstable on the surface.

As mentioned in the introduction, previous theoretical studies suggested a number of Ir-oxide phases that should exhibit OER activities greater than that of rutile $IrO_2$ employing the AEM mechanism as a computational screening framework.[16−18] We can see from Table 1, however, that this enhancement is concurrent with the activation of lattice oxygen atoms leading to substantially decreased overpotentials for the LOM pathways. This is not surprising as the analyzed $O_{cus}$ and $O_{lat}$ reaction sites (see Figure 1) share the same transition-metal centers. Lattice oxygen participation in the OER should have important implications for electrochemical stability of Ir-oxides. It is seen from Table 1 that LOM2 features quite high overpotentials across Ir-oxides that are likely related to the inaccessibility of the $O_{lat}$ sites for water nucleophilic attack for the ideal defect-free oxide surfaces. On the other hand, LOM1 can exhibit thermodynamic overpotentials as low as AEM as found for the $R\bar{3}c$ and $Pm\bar{3}m$ prototypes. Furthermore, in the case of $Pm\bar{3}m$ we consistently observed the detachment of Ir from the surface when optimizing some OER structures in static DFT or equilibrating in AIMD. This suggests that this phase is unlikely to be stable under the OER conditions.

During the last few decades, considerable efforts have been put into identifying simple descriptors based on electronic-structure properties that can be used to predict electrocatalytic activities of materials.[7] Among them, p and d band centers turned out to be rather successful. In the case of the OER electrocatalysis, it was shown that the O 2p-band center can be well correlated with the OER activities.[51] For instance, it was revealed in the example of perovskite oxides that the closer the O 2p-band center is to the Fermi level, the greater the OER activity.[52] This was attributed to the metal-oxide covalency that can be quantified as the energy difference between the band centers for the occupied O 2p band and unoccupied transition-metal 3d band. It is also clear that if the O 2p-band center is too close to the Fermi level, then it should destabilize the oxide lattice because of the lattice oxygen evolution reaction. Recently, we have successfully used the O 2p-band center as a descriptor to predict highly OER active surface configurations of rutile $RuO_2$ and $IrO_2$ in the presence of transition-metal vacancies.[38] Here, we also show that it can be used as a crude descriptor to analyze OER activities toward both the AEM and LOM pathways across different Ir oxides (see section 3 in the Supporting Information).

We next carry out an *ab initio* thermodynamic analysis of the OER in the presence of surface Ir vacancies. Such metal vacancies can be formed during electrochemical dissolution and are known to promote OER reactivity.[38,53,54] For example, it was shown for the $IrNiO_x$ nanoparticles that Ni leaching gives rise to the formation of surface Ir vacancies.[53] Consequently, oxygen ions adjacent to the metal vacancies increase their hole character which in turn leads to more positive oxidation states of Ir than the formal 4+ in stoichiometric $IrO_2$. From the electronic structure point of view, this should lower the Ir 5d states below the O 2p states, resulting in significant oxygen hole character. It was then hypothesized that the electrophilic character of these oxygen ligands may lead to reduced kinetic barriers for nucleophilic O−O bond formation. In this section we explore OER thermodynamics toward both the AEM and LOM mechanisms for vacancy-containing Ir-oxide surfaces, while in the next section we directly evaluate kinetic barriers of the OER processes.

We focus here on the pyrite $IrO_2$ and $\alpha$-$IrO_3$ phases as representative cases of pure Ir oxides and compare them with the state-of-the-art rutile $IrO_2$. For these three polymorphs we systematically examine OER thermodynamics considering surface models with 1−4 Ir vacancies around the reaction site. Armed with the O 2p-band center as a descriptor, we used it to identify the most promising (*i.e.*, with the lowest OER overpotentials) structural configurations involving Ir vacancies. It should be noted that because the O 2p-band center is not a perfect descriptor, we cannot rule out that other configurations not considered here may exhibit even more favorable OER thermodynamics.


https://dx.doi.org/10.1021/acsenergylett.1c00234
ACS Energy Lett. 2021, 6, 1124−1133

Table 2 reports the values of the OER overpotentials for the rutile, pyrite, and $\alpha$-$IrO_3$ surfaces as a function of the number of Ir vacancies. The corresponding atomic structures are shown in Figure S3. It is clearly seen from the table that as the number of vacancies is increased, the LOM mechanisms become more competitive with AEM for all oxides. It turns out that in some cases LOM1 is thermodynamically more favorable than both AEM and LOM2 featuring very low theoretical overpotentials. It is important to note that although we systematically address only mononuclear LOM pathways in this work, we were able to observe an alternative binuclear mechanism of LOM in our simulations. Specifically, we observed spontaneous formation of $O_2$ via binuclear LOM1 involving $O_{lat}-O_{lat}$ coupling between two adjacent $IrO_6$ octahedra for the four-vacancy model of $\alpha$-$IrO_3$ when optimizing some OER intermediates. Moreover, this process of $O_2$ formation was accompanied by detachment of Ir species from the surface (as $IrO_4$ units) even in static DFT calculations. We found that this became possible because of both high activity of lattice oxygen atoms and increased flexibility of $IrO_6$ units at the surface in the presence of Ir vacancies. This situation appears to be similar to the binuclear mechanism of AEM, also called the interaction of two M−O units (I2M), which was demonstrated to be favorable in certain cases such as, for example, nonstoichiometric $IrO_2$ films.[55,56]

**Table 2. Computed OER Overpotentials (in V) via AEM, LOM1, and LOM2 for the Rutile (110), Pyrite (100) and $\alpha$-$IrO_3$ (110) Surfaces Containing 1−4 Ir Vacancies**[a]

| structure | mechanism | 1-vac | 2-vac | 3-vac | 4-vac |
|---|---|---|---|---|---|
| rutile $IrO_2$ (110) | AEM | 0.60 | 0.35 | 0.18 | 0.26 |
| | LOM1 | 1.21 | 0.77 | 0.24 | 0.05 |
| | LOM2 | 1.33 | 1.12 | 0.24 | 0.22 |
| pyrite $IrO_2$ (100) | AEM | 0.35 | 0.45 | 0.53 | 0.64 |
| | LOM1 | 0.13 | 0.22 | 0.19 | 0.33 |
| | LOM2 | 1.04 | 1.11 | 0.98 | 0.62 |
| $\alpha$-$IrO_3$ (110) | AEM | 0.26 | 0.55 | 0.52 | |
| | LOM1 | 0.31 | 0.55 | 0.52 | * |
| | LOM2 | 0.34 | 0.78 | 0.62 | |

[a]The corresponding structural models are provided in Figure S3. In the case of the four-vacancy surface model for $\alpha$-$IrO_3$, we detect spontaneous $O_2$ formation during DFT optimization following the binuclear LOM1 mechanism (*).

We point out here that the investigated structural models with Ir vacancies obviously cannot represent the whole diversity of OER active sites that can form during electrochemical dissolution/corrosion. Nevertheless, we have recently shown[38] that the observed trend of LOM becoming competitive with AEM is preserved even if more complex structures with undercoordinated surface atoms are analyzed. Specifically, we demonstrated this on the example of the rutile-type $MO_2$(121) (M = Ru, Ir) double kinks that are believed to play an important role in materials dissolution. Overall, the obtained theoretical results indicate that the thermodynamic driving force for the LOM pathways becomes more favorable in the presence of electrophilic oxygen species at the Ir-oxide surfaces, in agreement with experimental claims.[33,35,36,53]

One of the important limitations of the CHE approach is a lack of information about kinetic barriers of electrocatalytic reactions. While the Brønsted−Evans−Polanyi (BEP) principle stating the linear relationship between the activation energy and the enthalpy of reaction is useful, it would be better to estimate activation barriers explicitly. In relation to the OER mechanisms explored in this study, it would be instrumental to answer the following questions: (1) Can the LOM mechanisms win over AEM not only thermodynamically but also kinetically? This is especially interesting to know when thermodynamic overpotentials for different reaction pathways turn out to be very close. (2) Which of the two LOM pathways (involving O−O coupling or water attack) should be kinetically more favorable? With these questions in mind, we next examine the kinetics of the AEM and LOM mechanisms utilizing AIMD-based blue moon ensemble simulations with explicit treatment of water environment at room temperature.

It is established theoretically that the potential-determining step (PDS) of AEM across a variety of oxides including $RuO_2$- and $IrO_2$-based systems is either the water attack or $O_2$ desorption reaction step (see Scheme 1).[16,17,20] It is believed that the detachment of neutral $O_2$ being a purely chemical reaction is unlikely to be the rate-determining step of the overall OER process.[57] However, this issue remains unsettled based on prior thermodynamic analyses and will be addressed as part of our kinetic modeling. Thus, we will examine here the kinetics of both reaction steps.

In terms of the systems, we choose to contrast the benchmark rutile (110) surface with the pyrite (100) surface in the presence of three and four Ir vacancies. Our motivation for this choice is that according to the OER thermodynamics we can expect favorable kinetics for both the LOM1 and LOM2 pathways. In the case of $\alpha$-$IrO_3$ we have already observed spontaneous formation of $O_2$ through the binuclear LOM1 mechanism in static DFT calculations. Because of the computational cost associated with accurate AIMD kinetic simulations, we adopt the following approach. To obtain a crude estimate of kinetic barriers for the AEM, LOM1, and LOM2 pathways, we first commence computationally efficient slow-growth simulations for both the three- and four-vacancy models of rutile and pyrite. This allows us to check whether the three- and four-vacancy systems exhibit qualitatively the same behavior. Then, we perform blue moon ensemble simulations for the three-vacancy surfaces of rutile and pyrite to obtain accurate estimates of the corresponding reaction barriers. A statistical error analysis utilizing the block averaging method is carried out to evaluate the uncertainty of AIMD-derived activation barriers (see the Supporting Information).

A comment on the accuracy of both DFT-based thermodynamic and kinetic calculations of the OER is in order. It is well-known that the semilocal functionals such as RPBE employed in this study overestimate the formation energy of $O_2$(gas) (overbinding).[21,25] The standard workaround in DFT-based CHE calculations of OER overpotentials is to introduce an *ad hoc* correction by using the experimental value for the OER free energy ($\Delta G_{OER}^{exp}$ = 4.92 eV). As a result, the ideal catalyst should exhibit four equidistant steps with $\Delta G$ = 1.23 eV ($\eta_{OER}$ = 0 V) as calculated by DFT for the conventional reaction mechanism. Although not perfect as different reaction steps can suffer from the error to a varying degree, the approach has been widely used in first-principles electrocatalysis, including the present work. In our AIMD free energy simulations of OER activation barriers using the RPBE functional we are not introducing any experimental correction. This allows us to consistently contrast kinetic barriers between


https://dx.doi.org/10.1021/acsenergylett.1c00234
ACS Energy Lett. 2021, 6, 1124−1133

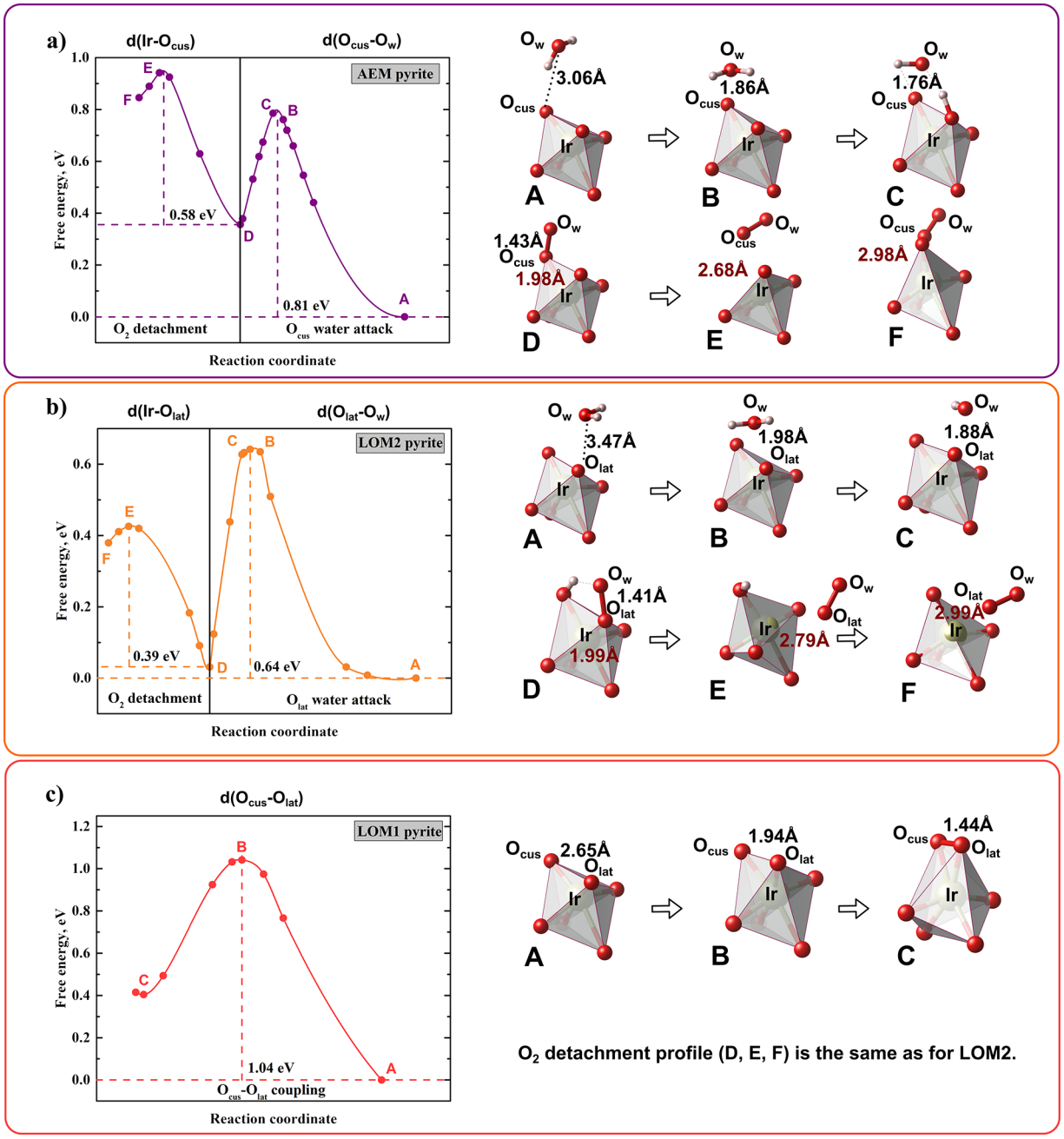


**Figure 2. Free-energy profiles from AIMD thermodynamic integration simulations for $O_2$ formation and desorption steps along the AEM (a), LOM2 (b), and LOM1 (c) pathways over the pyrite (100) surface with three Ir vacancies (see the atomic structure in Figure S3). Atomic structures of the intermediate states with the distances along two collective variables are also presented. We note that for both AEM and LOM2 the first proton from attacking $H_2O$ spontaneously adsorbs on the adjacent $O_{cus}$ site, while the second proton is either transferred to solution for AEM or occupies the same $O_{cus}$ site for LOM2.**

the AEM and LOM mechanisms, but this makes it hard to compare the obtained results with DFT thermodynamic data.

Another important difference between our DFT thermodynamics and kinetics data is the absence of solvent effects in the adsorbate binding energies estimated within the CHE approach. While incorporation of implicit solvation corrections in DFT thermodynamics is possible,[58−60] it is unclear what dielectric constants for water need be adopted when considering surfaces with different structure and chemistry (*e.g.*, with various number of Ir vacancies). This is the reason why we refrained from using the implicit solvent approach in our calculations of thermodynamic overpotenials. Regarding the explicit treatment of water environment, it was demonstrated that the computed adsorption energies of reaction intermediates with and without explicit water molecules may differ quite significantly.[61] To provide some estimate of how large such a difference could be for our systems, we have run slow-growth simulations of the LOM2 water attack step on the example of the pyrite surface without Ir vacancies. We have determined the kinetic barrier of 0.9 eV with and 1.4 eV without the explicit water environment. The absolute values of these numbers are overestimated because of poor statistical sampling of such slow-growth simulations, but


https://dx.doi.org/10.1021/acsenergylett.1c00234
ACS Energy Lett. 2021, 6, 1124−1133

it does show the magnitude of the difference between two sets of calculations consistent with other theoretical estimates.[61]

Figures S4−S7 show the free energy profiles for the AEM, LOM1, and LOM2 pathways computed from AIMD slow-growth simulations. These results reveal that for both materials (rutile and pyrite) and for both structural models (three- and four-vacancy) the LOM1 mechanism exhibits consistently higher activation barriers than LOM2. This is expected as LOM1 involving the O−O coupling at the same metal site proceeds via a highly strained transition state. Another general observation is that the activation barriers estimated from slow growth for both materials tend to decrease upon increasing the number of Ir vacancies, in overall agreement with DFT thermodynamics. Below, we focus on only the three-vacancy systems using the more accurate blue moon approach.

Figures 2 and S8 show the free energy profiles derived from AIMD thermodynamic integration for all three OER mechanisms for the three-vacancy pyrite and rutile systems, respectively. In these calculations we employ separate collective variables (CVs) for each reaction step ($O_2$ formation and $O_2$ desorption). For the water attack reactions we use the distance between a surface O atom (either $O_{cus}$ or $O_{lat}$) and an O atom from solution $H_2O$ as CVs denoted as $d(O_{cus}-O_w)$ and $d(O_{lat}-O_w)$ for the AEM and LOM2 mechanisms, respectively. For LOM1 we use the distance between $O_{cus}$ and $O_{lat}$ as a CV denoted as $d(O_{cus}-O_{lat})$. For the $O_2$ desorption step we employ the distance between the surface Ir atom and O atom leaving the surface as part of the newly formed $O_2$ molecule denoted as $d(Ir-O_{cus})$ and $d(Ir-O_{lat})$ for the AEM and LOM2 mechanisms, respectively. In the case of LOM1, desorption of $O_2$ will have the same barrier as in LOM2 after Ir has satisfied its missing valence by adsorbing OH from solution. Characteristic interatomic distances corresponding to a set of intermediate points along each free energy profile are also shown in the figures.

It is clearly seen for both rutile and pyrite that LOM2 exhibits activation barriers almost twice lower than LOM1 suggesting water attack as a more favorable LOM pathway. These results are qualitatively consistent with the slow-growth data obtained for both three- and four-vacancy models (see Figures S4−S7). Also, we observe that while for rutile AEM remains preferred over LOM2 even in the case of three Ir vacancies on the surface (0.54 eV vs 0.66 eV), LOM2 becomes more favorable than AEM for defective pyrite (0.64 eV vs 0.81 eV). This suggests that LOM2 can indeed outperform AEM even if the uncertainties of statistical sampling are taken into account (see the Supporting Information). Specifically, we determine that the uncertainties in computed activation barriers do not exceed 8% (see Table S2). Our kinetic modeling also reveals for both rutile and pyrite that it is the water attack and not the desorption of $O_2$ that should be the rate-determining step, thus directly supporting previous claims.

In summary, the obtained results allow us to answer the questions raised earlier: (1) LOM can indeed outperform AEM both thermodynamically and kinetically for certain surface structures involving Ir vacancies, and (2) among the two lattice oxygen mechanisms LOM2 (water attack) turns out to be substantially more favorable than mononuclear LOM1 (O−O coupling) from the kinetics point of view. However, we note that we have also observed spontaneous binuclear LOM1 reaction in the case of defective $\alpha$-$IrO_3$ as discussed earlier. Overall, the results indicate that different LOM mechanisms can be attainable in Ir-oxides, but the degree of their involvement in the OER process should depend on materials chemistry. We believe that the obtained insights in the competition between AEM and LOM could be generalized to metal-oxide electrocatalysts beyond Ir-based examples.

Having established high AEM and LOM activities of pure Ir-oxide phases both thermodynamically and kinetically, we also want to explore whether doped Ir-oxide systems should exhibit a similar activation of lattice oxygen atoms. This is important because doping is a viable strategy to enhance the activity of OER electrocatalysts while at the same time decreasing their cost. Recently, such binary oxide systems have been examined both theoretically[17] and experimentally[53,62] with regard to their OER performance. Here, we pick a number of equimolar bimetallic Ir-based oxides adopting the same atomic arrangements as in a previous DFT study.[17] In addition to favorable OER activities, these systems were shown to be electrochemically stable according to the computed Pourbaix diagrams. Our results discussed in detail in section 9 of the Supporting Information reinforce the above findings for the pure Ir-oxide phases. Specifically, we show that enhancement of the OER activity via AEM is concurrent with the activation of lattice oxygen atoms toward LOM in the doped systems as well. Thus, lattice oxygen evolution reaction across all the studied systems is expected that should compromise their electrochemical stability.

In summary, we have conducted a theoretical analysis of the OER activity of Ir-bearing oxides through a combination of DFT-based thermodynamic and kinetic calculations. The study demonstrates that for a variety of $IrO_2$, $IrO_3$, and bimetallic $IrO_2$-based phases the activation of lattice oxygen atoms toward $O_2$ evolution is concurrent with high activity of terminal oxygen atoms involved in the conventional OER mechanism. Importantly, as the number of surface defects (Ir vacancies) is increased, the lattice oxygen mechanism (LOM) can outperform the conventional adsorbate evolving mechanism (AEM). This is supported by both DFT calculations of reaction free energies and AIMD simulations of reaction activation barriers. The results suggest that among pure Ir-oxide polymorphs rutile $IrO_2$ should be least susceptible to the lattice oxygen involvement in agreement with its superior OER stability. Of all the equimolar bimetallic oxides examined in this work, Ti−$IrO_2$ is identified as the system least prone toward the lattice oxygen evolution at the same time featuring OER activities comparable to that of rutile $IrO_2$. This is consistent with newly published experimental data showing the promising OER activity/stability properties of Ti−$IrO_2$.

For the mononuclear LOM mechanism we have examined two major reaction pathways: the one involving O−O coupling and the other involving nucleophilic water attack. The activation barriers estimated from AIMD thermodynamic integration on the example of rutile and pyrite surfaces containing Ir vacancies indicate that the water attack pathway is kinetically more favorable. However, we have also observed spontaneous formation of $O_2$ from lattice oxygen atoms in the case of $\alpha$-$IrO_3$ in the presence of Ir vacancies following the binuclear mechanism sometimes also called the interaction of two M−O units (I2M). Further more systematic investigations are required to better understand the energetics of different lattice oxygen mechanisms as a function of materials chemistry.

Overall, the obtained results suggest that the enhanced OER activity of Ir-based oxides relative to rutile $IrO_2$ should come at the expense of their electrochemical stability because of the involvement of lattice oxygen in the reaction. Other studies are


https://dx.doi.org/10.1021/acsenergylett.1c00234
ACS Energy Lett. 2021, 6, 1124−1133

warranted to quantify the degree to which lattice oxygen participation can compromise stability of OER catalysts in practice. This work accentuates the importance of the lattice oxygen evolution reaction for electrochemical stability of oxides in addition to commonly used Pourbaix stability analyses. More specifically, the results suggest that computational design of efficient OER electrocatalysts should identify new chemistries with favorable uncoupling between AEM and LOM to improve activity-stability trade-off.

## ■ ASSOCIATED CONTENT

### Supporting Information

The Supporting Information is available free of charge at https://pubs.acs.org/doi/10.1021/acsenergylett.1c00234.

Computational details; atomic structures of $IrO_2$ and $IrO_3$ systems; partial density of states; free energy profiles from slow-growth simulations of OER reaction barriers for rutile and pyrite surfaces; DFT free energies for OER reactions for rutile, pyrite, and $R\bar{3}c$ $IrO_3$ surfaces as a function of Ir vacancies; statistical error analysis; electrode potential estimation; and the results for transition-metal doped $IrO_2$ (PDF)

Movies of the OER reaction trajectories on the example of the rutile (110) surface with three Ir vacancies (ZIP)

Exemplary VASP input files for blue moon calculations of the OER over the rutile (110) surface with three Ir vacancies (ZIP)

## ■ AUTHOR INFORMATION


### Corresponding Author

**Vitaly Alexandrov** − *Department of Chemical and Biomolecular Engineering and Nebraska Center for Materials and Nanoscience, University of Nebraska—Lincoln, Lincoln, Nebraska 68588, United States;* orcid.org/0000-0003-2063-6914; Phone: +1 (402) 472-5323; Email: valexandrov2@unl.edu; Fax: +1 (402) 472-6989

### Authors

**Alexandra Zagalskaya** − *Department of Chemical and Biomolecular Engineering, University of Nebraska—Lincoln, Lincoln, Nebraska 68588, United States*

**Iman Evazzade** − *Department of Chemical and Biomolecular Engineering, University of Nebraska—Lincoln, Lincoln, Nebraska 68588, United States*

Complete contact information is available at: https://pubs.acs.org/10.1021/acsenergylett.1c00234

### Author Contributions

¶A.Z. and I.E. contributed equally to this work


### Notes

The authors declare no competing financial interest.

## ■ ACKNOWLEDGMENTS

We acknowledge funding support from the National Science Foundation (NSF) through the NSF CAREER award (Grant No. CBET-1941204). This research used resources of the National Energy Research Scientific Computing Center, a DOE Office of Science User Facility supported by the Office of Science of the U.S. Department of Energy under Contract No. DE-AC02-05CH11231, as well as the Holland Computing Center at the University of Nebraska—Lincoln.

## ■ REFERENCES


(1) Calle-Vallejo, F.; Koper, M. T. First-principles computational electrochemistry: Achievements and challenges. *Electrochim. Acta* **2012**, *84*, 3−11.

(2) Katsounaros, I.; Cherevko, S.; Zeradjanin, A. R.; Mayrhofer, K. J. J. Oxygen Electrochemistry as a Cornerstone for Sustainable Energy Conversion. *Angew. Chem., Int. Ed.* **2014**, *53*, 102−121.

(3) McCrory, C. C. L.; Jung, S.; Ferrer, I. M.; Chatman, S. M.; Peters, J. C.; Jaramillo, T. F. Benchmarking Hydrogen Evolving Reaction and Oxygen Evolving Reaction Electrocatalysts for Solar Water Splitting Devices. *J. Am. Chem. Soc.* **2015**, *137*, 4347−4357.

(4) Burke, M. S.; Enman, L. J.; Batchellor, A. S.; Zou, S.; Boettcher, S. W. Oxygen Evolution Reaction Electrocatalysis on Transition Metal Oxides and (Oxy)hydroxides: Activity Trends and Design Principles. *Chem. Mater.* **2015**, *27*, 7549−7558.

(5) Fabbri, E.; Schmidt, T. J. Oxygen Evolution Reaction—The Enigma in Water Electrolysis. *ACS Catal.* **2018**, *8*, 9765−9774.

(6) Busch, M. Water oxidation: From mechanisms to limitations. *Current Opinion in Electrochemistry* **2018**, *9*, 278−284.

(7) Song, J.; Wei, C.; Huang, Z.-F.; Liu, C.; Zeng, L.; Wang, X.; Xu, Z. J. A review on fundamentals for designing oxygen evolution electrocatalysts. *Chem. Soc. Rev.* **2020**, *49*, 2196−2214.

(8) Cherevko, S.; Reier, T.; Zeradjanin, A. R.; Pawolek, Z.; Strasser, P.; Mayrhofer, K. J. Stability of nanostructured iridium oxide electrocatalysts during oxygen evolution reaction in acidic environment. *Electrochem. Commun.* **2014**, *48*, 81−85.

(9) Geiger, S.; Kasian, O.; Ledendecker, M.; Pizzutilo, E.; Mingers, A. M.; Fu, W. T.; Diaz-Morales, O.; Li, Z.; Oellers, T.; Fruchter, L.; Ludwig, A.; Mayrhofer, K. J. J.; Koper, M. T. M.; Cherevko, S. The stability number as a metric for electrocatalyst stability benchmarking. *Nature Catalysis* **2018**, *1*, 508−515.

(10) Zhang, Y.; Gao, L.; Hensen, E. J. M.; Hofmann, J. P. Evaluating the Stability of $Co_2P$ Electrocatalysts in the Hydrogen Evolution Reaction for Both Acidic and Alkaline Electrolytes. *ACS Energy Letters* **2018**, *3*, 1360−1365.

(11) Bae, D.; Seger, B.; Vesborg, P. C. K.; Hansen, O.; Chorkendorff, I. Strategies for stable water splitting via protected photoelectrodes. *Chem. Soc. Rev.* **2017**, *46*, 1933−1954.

(12) Göhl, D.; Garg, A.; Paciok, P.; Mayrhofer, K. J. J.; Heggen, M.; Shao-Horn, Y.; Dunin-Borkowski, R. E.; Román-Leshkov, Y.; Ledendecker, M. Engineering stable electrocatalysts by synergistic stabilization between carbide cores and Pt shells. *Nat. Mater.* **2020**, *19*, 287−291.

(13) Ruiz Esquius, J.; Algara-Siller, G.; Spanos, I.; Freakley, S. J.; Schlögl, R.; Hutchings, G. J. Preparation of Solid Solution and Layered $IrO_x$-$Ni(OH)_2$ Oxygen Evolution Catalysts: Toward Optimizing Iridium Efficiency for OER. *ACS Catal.* **2020**, *10*, 14640−14648.

(14) Persson, K. A.; Waldwick, B.; Lazic, P.; Ceder, G. Prediction of solid-aqueous equilibria: Scheme to combine first-principles calculations of solids with experimental aqueous states. *Phys. Rev. B: Condens. Matter Mater. Phys.* **2012**, *85*, 235438.

(15) Kim, B.-J.; Abbott, D. F.; Cheng, X.; Fabbri, E.; Nachtegaal, M.; Bozza, F.; Castelli, I. E.; Lebedev, D.; Schäublin, R.; Copéret, C.; Graule, T.; Marzari, N.; Schmidt, T. J. Unraveling Thermodynamics, Stability, and Oxygen Evolution Activity of Strontium Ruthenium Perovskite Oxide. *ACS Catal.* **2017**, *7*, 3245−3256.

(16) Back, S.; Tran, K.; Ulissi, Z. W. Toward a Design of Active Oxygen Evolution Catalysts: Insights from Automated Density Functional Theory Calculations and Machine Learning. *ACS Catal.* **2019**, *9*, 7651−7659.

(17) Back, S.; Tran, K.; Ulissi, Z. W. Discovery of Acid-Stable Oxygen Evolution Catalysts: High-Throughput Computational Screening of Equimolar Bimetallic Oxides. *ACS Appl. Mater. Interfaces* **2020**, *12*, 38256−38265.

(18) Flores, R. A.; Paolucci, C.; Winther, K. T.; Jain, A.; Torres, J. A. G.; Aykol, M.; Montoya, J.; Nørskov, J. K.; Bajdich, M.; Bligaard, T. Active Learning Accelerated Discovery of Stable Iridium Oxide

Polymorphs for the Oxygen Evolution Reaction. *Chem. Mater.* **2020**, *32*, 5854−5863.
(19) Man, I. C.; Su, H.-Y.; Calle-Vallejo, F.; Hansen, H. A.; Martínez, J. I.; Inoglu, N. G.; Kitchin, J.; Jaramillo, T. F.; Nørskov, J. K.; Rossmeisl, J. Universality in Oxygen Evolution Electrocatalysis on Oxide Surfaces. *ChemCatChem* **2011**, *3*, 1159−1165.
(20) Briquet, L. G. V.; Sarwar, M.; Mugo, J.; Jones, G.; Calle-Vallejo, F. A New Type of Scaling Relations to Assess the Accuracy of Computational Predictions of Catalytic Activities Applied to the Oxygen Evolution Reaction. *ChemCatChem* **2017**, *9*, 1261−1268.
(21) Gono, P.; Pasquarello, A. Oxygen evolution reaction: Bifunctional mechanism breaking the linear scaling relationship. *J. Chem. Phys.* **2020**, *152*, 104712.
(22) Gunasooriya, G. T. K. K.; Nørskov, J. K. Analysis of Acid-Stable and Active Oxides for the Oxygen Evolution Reaction. *ACS Energy Letters* **2020**, *5*, 3778−3787.
(23) Shan, J.; Zheng, Y.; Shi, B.; Davey, K.; Qiao, S.-Z. Regulating Electrocatalysts via Surface and Interface Engineering for Acidic Water Electrooxidation. *ACS Energy Letters* **2019**, *4*, 2719−2730.
(24) Yang, C.; Batuk, M.; Jacquet, Q.; Rousse, G.; Yin, W.; Zhang, L.; Hadermann, J.; Abakumov, A. M.; Cibin, G.; Chadwick, A.; Tarascon, J.-M.; Grimaud, A. Revealing pH-Dependent Activities and Surface Instabilities for Ni-Based Electrocatalysts during the Oxygen Evolution Reaction. *ACS Energy Letters* **2018**, *3*, 2884−2890.
(25) Yoo, J. S.; Rong, X.; Liu, Y.; Kolpak, A. M. Role of Lattice Oxygen Participation in Understanding Trends in the Oxygen Evolution Reaction on Perovskites. *ACS Catal.* **2018**, *8*, 4628−4636.
(26) Liu, J.; Jia, E.; Stoerzinger, K. A.; Wang, L.; Wang, Y.; Yang, Z.; Shen, D.; Engelhard, M. H.; Bowden, M. E.; Zhu, Z.; Chambers, S. A.; Du, Y. Dynamic Lattice Oxygen Participation on Perovskite $LaNiO_3$ during Oxygen Evolution Reaction. *J. Phys. Chem. C* **2020**, *124*, 15386−15390.
(27) Grimaud, A.; Diaz-Morales, O.; Han, B.; Hong, W. T.; Lee, Y.-L.; Giordano, L.; Stoerzinger, K. A.; Koper, M. T. M.; Shao-Horn, Y. Activating lattice oxygen redox reactions in metal oxides to catalyse oxygen evolution. *Nat. Chem.* **2017**, *9*, 457−465.
(28) Pan, Y.; Xu, X.; Zhong, Y.; Ge, L.; Chen, Y.; Veder, J.-P. M.; Guan, D.; O'Hayre, R.; Li, M.; Wang, G.; Wang, H.; Zhou, W.; Shao, Z. Direct evidence of boosted oxygen evolution over perovskite by enhanced lattice oxygen participation. *Nat. Commun.* **2020**, *11*, 2002.
(29) Rong, X.; Parolin, J.; Kolpak, A. M. A Fundamental Relationship between Reaction Mechanism and Stability in Metal Oxide Catalysts for Oxygen Evolution. *ACS Catal.* **2016**, *6*, 1153−1158.
(30) Mefford, J. T.; Rong, X.; Abakumov, A. M.; Hardin, W. G.; Dai, S.; Kolpak, A. M.; Johnston, K. P.; Stevenson, K. J. Water electrolysis on $La_{1x}Sr_xCoO_{3\delta}$ perovskite electrocatalysts. *Nat. Commun.* **2016**, *7*, 11053.
(31) Huang, Z.-F.; Song, J.; Du, Y.; Xi, S.; Dou, S.; Nsanzimana, J. M. V.; Wang, C.; Xu, Z. J.; Wang, X. Chemical and structural origin of lattice oxygen oxidation in Co-Zn oxyhydroxide oxygen evolution electrocatalysts. *Nature Energy* **2019**, *4*, 329−338.
(32) Danilovic, N.; Subbaraman, R.; Chang, K. C.; Chang, S. H.; Kang, Y.; Snyder, J.; Paulikas, A. P.; Strmcnik, D.; Kim, Y. T.; Myers, D.; Stamenkovic, V. R.; Markovic, N. M. Using Surface Segregation To Design Stable Ru-Ir Oxides for the Oxygen Evolution Reaction in Acidic Environments. *Angew. Chem., Int. Ed.* **2014**, *53*, 14016−14021.
(33) Grimaud, A.; Demortière, A.; Saubanère, M.; Dachraoui, W.; Duchamp, M.; Doublet, M.-L.; Tarascon, J.-M. Activation of surface oxygen sites on an iridium-based model catalyst for the oxygen evolution reaction. *Nature Energy* **2017**, *2*, 16189.
(34) Cherevko, S.; Geiger, S.; Kasian, O.; Kulyk, N.; Grote, J.-P.; Savan, A.; Shrestha, B. R.; Merzlikin, S.; Breitbach, B.; Ludwig, A.; Mayrhofer, K. J. Oxygen and hydrogen evolution reactions on Ru, $RuO_2$, Ir, and $IrO_2$ thin film electrodes in acidic and alkaline electrolytes: A comparative study on activity and stability. *Catal. Today* **2016**, *262*, 170−180.
(35) Kasian, O.; Geiger, S.; Li, T.; Grote, J.-P.; Schweinar, K.; Zhang, S.; Scheu, C.; Raabe, D.; Cherevko, S.; Gault, B.; Mayrhofer, K. J. J. Degradation of iridium oxides via oxygen evolution from the lattice: correlating atomic scale structure with reaction mechanisms. *Energy Environ. Sci.* **2019**, *12*, 3548−3555.
(36) Pfeifer, V.; et al. The electronic structure of iridium oxide electrodes active in water splitting. *Phys. Chem. Chem. Phys.* **2016**, *18*, 2292−2296.
(37) Schweinar, K.; Gault, B.; Mouton, I.; Kasian, O. Lattice Oxygen Exchange in Rutile $IrO_2$ during the Oxygen Evolution Reaction. *J. Phys. Chem. Lett.* **2020**, *11*, 5008−5014.
(38) Zagalskaya, A.; Alexandrov, V. Role of Defects in the Interplay between Adsorbate Evolving and Lattice Oxygen Mechanisms of the Oxygen Evolution Reaction in $RuO_2$ and $IrO_2$. *ACS Catal.* **2020**, *10*, 3650−3657.
(39) Binninger, T.; Mohamed, R.; Waltar, K.; Fabbri, E.; Levecque, P.; Kötz, R.; Schmidt, T. J. Thermodynamic explanation of the universal correlation between oxygen evolution activity and corrosion of oxide catalysts. *Sci. Rep.* **2015**, *5*, 12167.
(40) Grimaud, A.; Hong, W. T.; Shao-Horn, Y.; Tarascon, J.-M. Anionic redox processes for electrochemical devices. *Nat. Mater.* **2016**, *15*, 121−126.
(41) Saubanère, M.; McCalla, E.; Tarascon, J.-M.; Doublet, M.-L. The intriguing question of anionic redox in high-energy density cathodes for Li-ion batteries. *Energy Environ. Sci.* **2016**, *9*, 984−991.
(42) Li, M.; Liu, T.; Bi, X.; Chen, Z.; Amine, K.; Zhong, C.; Lu, J. Cationic and anionic redox in lithium-ion based batteries. *Chem. Soc. Rev.* **2020**, *49*, 1688−1705.
(43) Li, H.; Perez, A. J.; Taudul, B.; Boyko, T. D.; Freeland, J. W.; Doublet, M.-L.; Tarascon, J.-M.; Cabana, J. Elucidation of Active Oxygen Sites upon Delithiation of $Li_3IrO_4$. *ACS Energy Letters* **2021**, *6*, 140−147.
(44) Perdew, J. P.; Burke, K.; Ernzerhof, M. Generalized gradient approximation made simple. *Phys. Rev. Lett.* **1996**, *77*, 3865.
(45) Zhang, Y.; Yang, W. Comment on "Generalized gradient approximation made simple. *Phys. Rev. Lett.* **1998**, *80*, 890.
(46) Kresse, G.; Furthmüller, J. Efficient iterative schemes for ab initio total-energy calculations using a plane-wave basis set. *Phys. Rev. B: Condens. Matter Mater. Phys.* **1996**, *54*, 11169−11186.
(47) Kresse, G.; Furthmüller, J. Efficiency of ab-initio total energy calculations for metals and semiconductors using a plane-wave basis set. *Comput. Mater. Sci.* **1996**, *6*, 15−50.
(48) Nørskov, J. K.; Rossmeisl, J.; Logadottir, A.; Lindqvist, L.; Kitchin, J. R.; Bligaard, T.; Jónsson, H. Origin of the Overpotential for Oxygen Reduction at a Fuel-Cell Cathode. *J. Phys. Chem. B* **2004**, *108*, 17886−17892.
(49) Govindarajan, N.; Garcia-Lastra, J. M.; Meijer, E. J.; Calle-Vallejo, F. Does the breaking of adsorption-energy scaling relations guarantee enhanced electrocatalysis? *Current Opinion in Electrochemistry* **2018**, *8*, 110−117.
(50) Klyukin, K.; Rosso, K. M.; Alexandrov, V. Iron Dissolution from Goethite ($\alpha$-FeOOH) Surfaces in Water by Ab Initio Enhanced Free-Energy Simulations. *J. Phys. Chem. C* **2018**, *122*, 16086−16091.
(51) Dickens, C. F.; Montoya, J. H.; Kulkarni, A. R.; Bajdich, M.; Nørskov, J. K. An electronic structure descriptor for oxygen reactivity at metal and metal-oxide surfaces. *Surf. Sci.* **2019**, *681*, 122−129.
(52) Grimaud, A.; May, K. J.; Carlton, C. E.; Lee, Y.-L.; Risch, M.; Hong, W. T.; Zhou, J.; Shao-Horn, Y. Double perovskites as a family of highly active catalysts for oxygen evolution in alkaline solution. *Nat. Commun.* **2013**, *4*, 2439.
(53) Nong, H. N.; Reier, T.; Oh, H.-S.; Gliech, M.; Paciok, P.; Vu, T. H. T.; Teschner, D.; Heggen, M.; Petkov, V.; Schlögl, R.; Jones, T.; Strasser, P. A unique oxygen ligand environment facilitates water oxidation in hole-doped $IrNiO_x$ core-shell electrocatalysts. *Nature Catalysis* **2018**, *1*, 841−851.
(54) Zagalskaya, A.; Alexandrov, V. Mechanistic Study of $IrO_2$ Dissolution during the Electrocatalytic Oxygen Evolution Reaction. *J. Phys. Chem. Lett.* **2020**, *11*, 2695−2700.
(55) Fierro, S.; Nagel, T.; Baltruschat, H.; Comninellis, C. Investigation of the oxygen evolution reaction on Ti/$IrO_2$ electrodes


https://dx.doi.org/10.1021/acsenergylett.1c00234
*ACS Energy Lett.* 2021, 6, 1124−1133

using isotope labelling and on-line mass spectrometry. *Electrochem. Commun.* **2007**, *9*, 1969−1974.
(56) Klyukin, K.; Zagalskaya, A.; Alexandrov, V. Ab Initio Thermodynamics of Iridium Surface Oxidation and Oxygen Evolution Reaction. *J. Phys. Chem. C* **2018**, *122*, 29350−29358.
(57) Gauthier, J. A.; Dickens, C. F.; Chen, L. D.; Doyle, A. D.; Nørskov, J. K. Solvation Effects for Oxygen Evolution Reaction Catalysis on $IrO_2$(110). *J. Phys. Chem. C* **2017**, *121*, 11455−11463.
(58) Mathew, K.; Sundararaman, R.; Letchworth-Weaver, K.; Arias, T. A.; Hennig, R. G. Implicit solvation model for density-functional study of nanocrystal surfaces and reaction pathways. *J. Chem. Phys.* **2014**, *140*, 084106.
(59) Mathew, K.; Kolluru, V. S. C.; Mula, S.; Steinmann, S. N.; Hennig, R. G. Implicit self-consistent electrolyte model in plane-wave density-functional theory. *J. Chem. Phys.* **2019**, *151*, 234101.
(60) Basdogan, Y.; Maldonado, A. M.; Keith, J. A. Advances and challenges in modeling solvated reaction mechanisms for renewable fuels and chemicals. *WIREs Computational Molecular Science* **2020**, *10*, No. e1446.
(61) Rendón-Calle, A.; Builes, S.; Calle-Vallejo, F. Substantial improvement of electrocatalytic predictions by systematic assessment of solvent effects on adsorption energies. *Appl. Catal., B* **2020**, *276*, 119147.
(62) Kasian, O.; Li, T.; Mingers, A. M.; Schweinar, K.; Savan, A.; Ludwig, A.; Mayrhofer, K. J. J. Stabilization of an iridium oxygen evolution catalyst by titanium oxides. *J. Phys.: Energy* **2020**, DOI: 10.1088/2515-7655/abbd34.


https://dx.doi.org/10.1021/acsenergylett.1c00234
*ACS Energy Lett.* 2021, 6, 1124−1133